Proceedings of ASME Turbo Expo 2011
GT2011
June 6-10, 2011, Vancouver, British Columbia, Canada

GT2011-45222

EFFECT OF THE AXIAL SPACING BETWEEN VANES AND BLADES ON THE PERFORMANCE OF A TRANSONIC AXIAL TURBINE

Dongil Chang
University of Ottawa
Mechanical Engineering
Ottawa, ON Canada
dchang@uottawa.ca

Stavros Tavoularis
University of Ottawa
Mechanical Engineering
Ottawa, ON Canada
stavros.tavoularis@uottawa.ca

ABSTRACT

Unsteady numerical simulations have been conducted to investigate the effect of axial spacing between the stator vanes and the rotor blades on the performance of a transonic, single-stage, high-pressure, axial turbine. Three cases were considered, the reference case, which is based on the geometry of a commercial jet engine and has an axial spacing at 50% blade span equal to 42% of the vane axial chord, as well as two other cases with axial spacings equal to 31 and 52% vane axial chords, respectively. Present interest has focused on the effect of axial gap size on the instantaneous and time-averaged flows as well as on the blade loading and the turbine performance. Decreasing the gap size reduced the pressure and increased the Mach number in the core flows in the gap region. However, the flows near the two endwalls did not follow monotonic trends with the gap size change; instead, the Mach numbers for both the small gap and the large gap cases were lower than that for the reference case. This Mach number decrease was attributed to increased turbulence due to the increased wake strength for the small gap case and the increased wake width for the large gap case. In all considered cases, large pressure fluctuations were observed in the front region of the blade suction sides. These pressure fluctuations were strongest for the smaller spacing. The turbine efficiencies of the cases with the larger and smaller spacings were essentially the same, but both were lower than that of the reference case. The stator loss for the smaller spacing case was lower than the one for the larger spacing case, whereas the opposite was true for the rotor loss.

NOMENCLATURE

A	Cross-sectional area
a	Magnitude of discrete Fourier transform
c_b	Blade axial chord
c_v	Vane axial chord
f	Frequency
h	Enthalpy
M	Mach number
P	Pressure
R	Specific gas constant
s	Specific entropy
T	Temperature
t	Time
t_b	Blade passing period
t_v	Vane passing period
V	Velocity
x,y,z	Co-ordinate axes for plots

Greek Symbols

ζ	Loss coefficient
η_{tt}	Total-to-total efficiency
ρ	Density
τ	Torque

Subscripts

r	Relative property in the rotating reference frame
s	Static property
0	Total property
1	Mass-weighted average at stator inlet
2	Mass-weighted average at stator-rotor interface
3	Mass-weighted average at rotor outlet

Acronyms

CFD	Computational Fluid Dynamics
HPT	High-pressure turbine
LPT	Low-pressure turbine
PS	Pressure side
SS	Suction side
SST	Shear Stress Turbulence
URANS	Unsteady Reynolds-averaged Navier-Stokes

INTRODUCTION

In gas turbines, an axial gap necessarily exists between blade rows of compressors and turbines. The determination of an optimum gap size is one of the crucial design considerations for aircraft engines, because this dimension not only affects the size and weight of the engine, but also its performance and the blade life. In this paper, we focus on high-pressure turbines.

At first glance, it seems obvious that the axial gap size must be kept as small as possible for the engine to be relatively small and light. However, reducing drastically the gap size would produce strong unsteady pressure fluctuations near the leading edges of blades and the trailing edges of the vanes. In transonic high-pressure turbines (HPT), these fluctuations are mostly the result of potential interactions (shock waves and pressure wave reflections) between the rotor and the stator and may introduce excessive vibrational stresses on the blades, thus causing material fatigue and shortening the blade life. When a small turbine size is not an essential requirement, as in the case of turbines operating on ground and sea, a moderate increase of gap size for better turbine performance would be acceptable. As the axial gap size is increased, the flow uniformity at the rotor inlet would be improved, because a larger spacing would allow a better mixing of the three-dimensional (3-D) flows induced by the radial pressure gradient and periodic stator-rotor interactions due to vane wakes and/or shocks. Nevertheless, an increased uniformity level at the rotor inlet is not necessarily beneficial for the turbine performance (Gaetani et al. [1]).

Dring et al. [2] were the first to examine experimentally the influence of axial gap size on the surface pressure and the heat transfer on the blade of a subsonic HPT. The turbine consisted of a stator with 22 vanes and a rotor with 28 blades. They performed their experiment in a large test rig, which allowed them to scale their turbine model to five times an actual turbine size. The turbine rotational speed was 410 rpm and the aspect ratios (i.e., height-to-axial chord length ratios) of the vanes and blades were 1.3 and 0.96, respectively. The compressibility effect was negligible as the turbine exit Mach number was 0.2. They considered two gap sizes, respectively equal to 35 and 65% of the vane axial chord. They measured surface pressure at mid-span of a blade and observed an increase of pressure fluctuations and the heat transfer coefficient as the gap size was reduced.

Koya and Kotake [3] performed unsteady 3-D Euler simulations of a HPT with axial gap sizes equal to 25 and 45% of the vane axial chord. There were 52 vanes in the stator and 68 blades in the rotor. The aspect ratios of the vanes and blades were respectively 0.5 and 1.3. They reported that the variations of flow angle and pressure increased as the gap size was decreased.

Venable et al. [4] measured pressure on the vane and blade surfaces of a transonic HPT at midspan for three axial gap sizes corresponding to 20, 40 and 60% of the vane axial chord. The turbine had 30 vanes and 45 blades. The vane's aspect ratio was 0.7, while the blade's aspect ratio was 1.1. The average rotational speed of the blades was 11796 rpm. Their experiment was conducted in a short-duration shock tunnel. The measurements were compared with predictions using 2- and 3-D unsteady Reynolds-averaged Navier-Stokes (URANS) solvers with the Baldwin-Lomax algebraic turbulence model. They reported that calculations of the pressure and the pressure envelope using the 3-D solver were in better agreement with their measurements than those using the 2-D solver. However, both solvers over-predicted the time-averaged pressure in the front part of the vane suction surface and under-predicted it on the blade suction surface toward the trailing edge. They reported that the pressure fluctuation near the blade leading edge increased as the gap size was decreased. They further investigated the gap size effect on turbine performance. Comparisons were made solely by numerical simulations. They presented performance data obtained using 2-D and 3-D solvers, but we will discuss only the 3-D simulation results because of their higher accuracy. They found that the efficiencies for the 40 and 60% gap cases were essentially the same and 1% higher than the efficiency for the 20% gap case. In a companion paper, Busby et al. [5] presented time-resolved pressure measurements. The variation of the time-resolved pressures at selected chordwise locations on the vane and the blade surfaces were compared with data from 2-D and 3-D simulations. Again, the 3-D simulations showed a better agreement with the experiment, indicating the importance of considering 3-D flow features, like vortices, shocks and wakes. Finally, they explained the small difference in the predicted turbine efficiencies and concluded that, as the gap size was decreased, the vane total pressure loss decreased, whereas the blade relative total pressure loss increased.

Gaetani et al. [1], [6] conducted two sets of subsonic HPT experiments in a closed-loop test rig: steady flow measurements using a five-hole probe [1] and unsteady flow measurements using a fast probe [6]. The turbine consisted of 22 vanes having an aspect ratio of 1.6 and 25 blades with an aspect ratio of 1.1. The rotational speed of the rotor was set to 6800 rpm. The vane exit Mach number was 0.55. They examined two cases with axial gaps equal to 35 and 100% of the vane axial chord, respectively. The case with the larger gap was chosen as an ideal case for low stator interference on the downstream rotor. In the steady measurements, stator secondary vortices for the 35% configuration were detected downstream of the rotor, whereas no such vortices were detected for the 100% configuration. The measured turbine efficiency in the 100% configuration was 4% lower than that in the 35% configuration. These authors explained that the higher loss for the 100% configuration was due to the combined effects of a thick end-wall boundary layer in the gap region and the high underturning downstream of the rotor. In the unsteady measurements, it was found that the time-resolved relative total pressure on a cross plane located downstream of the blade below mid-span were much stronger for the 35% configuration.

Kikuchi et al. [7] conducted experimental and numerical studies of a single-stage HPT employing a 3-D URANS solver with the k-ω model for three axial gap sizes equal to 25.5, 38.3, and 51.0% of the vane axial chord, respectively. The turbine had 50 vanes and 68 blades, while the aspect ratios for the vanes and blades were about 1.3 and 2.1, respectively. The aspect ratio for the blade was high, compared to values mentioned previously, because this turbine had been developed for a steam turbine engine. The turbine rotational speed was set to 1300 rpm. This study showed that the turbine efficiency increased with decreasing gap size and also that the measured efficiency increase was twice as large as the predicted one.

Yamada et al. [8] performed measurements similar to the ones by Kikuchi et al. [7] but their findings were different from those of Kikuchi et al. When they increased the rotational speed to 1650 rpm and considered slightly different gap sizes (24.6, 36.9, and 49.3% of the vane axial chord), the measured efficiencies with the smaller and middle gap size were the same, but both were higher than that for the larger spacing. In all considered cases, the differences in efficiency were less than 0.3%, which implies that the influence of the axial gap is very weak.

Gaetani et al. [9] repeated measurements conducted earlier by Gaetani et al. [1] using a case with the same nominal gap size (35% of the vane axial chord), but also considering two additional cases with gap sizes equal to 16 and 50% of the vane axial chord, respectively. To explain the transport of entropy within the rotor, they also conducted 2-D URANS simulations using FLUENT with the SST (Shear Stress Transport) turbulence model. The measurements indicated that the middle gap case had the highest efficiency, and that the efficiencies for the smaller and the larger gaps were essentially the same and approximately 1.2% lower than the efficiency of the nominal configuration. There was a strong radial variation in the measured efficiency for all three axial gap cases.

Yao and Carson [10] conducted a numerical simulation using the GE (General Electric) version of the MSU-Turbo URANS code to investigate the interactions between a HPT and a low-pressure turbine (LPT) and to evaluate the effect of the inter-turbine spacing change. They explained the aerodynamic loss mechanisms in the inter-turbine space between the HPT and the LPT, which includes the flow structures within the inter-turbine space, the effect of HPT nozzle wake on the loss, and the loss transfer to the LPT. Although they did not investigate the effect of the axial gap size change within the HPT, they provided valuable insight on the mechanisms by which the HPT stator vane wakes affect the LPT performance.

Based on this brief review, one may conjecture that the trend of HPT performance as the axial gap size is changed depends on the turbine geometry and rotational speed. This survey also shows that the only available axial gap study on a transonic, low-aspect ratio HPT is the experimental and computational study by Venable et al. [4] and Busby et al. [5]. The geometry and operating conditions in that study were different from those in the present one. In particular, in the previous work the rotational speed was 24% of ours and the vane number was twice the present one, whereas the blade number was close to the present one. It would therefore be of interest to investigate whether these differences would affect the dependence of HPT performance and flow features (shocks, wakes and vortices) on the axial gap size. In addition, blades for commercial high-pressure turbines have three-dimensional profiles, achieved by using different airfoil stacking methods, like leaning, bowing or sweeping; such designs improve flow uniformity downstream of the rotor by enforcing an appropriate radial distribution of the flow angle (Joslyn and Dring, [10]), but also affect the time-averaged and fluctuating pressure loading of the blade (Gaetani et al., [6]). Because, unlike blades used in previous studies, the blades of the transonic high-pressure turbine considered in this study had a three-dimensional profile and a low aspect ratio, it is uncertain whether the different trends in turbine performance and pressure loading observed by previous authors would apply to the present case as well. Thus, it seems worthwhile to make a comparative study of axial gap effects using a realistic model the specific device.

The present article describes the results of 3-D unsteady simulations of flows in a single-stage, high-pressure, transonic turbine with three different axial gap sizes between the stator vanes and the rotor blades. These results were evaluated comparatively to determine the effects of axial gap size on turbine performance, pressure loadings on blades, as well as local flow features within the gap region. The cases considered were a reference case, having an axial gap equal to 42% of the vane axial chord and previously discussed by Chang and Tavoularis [12], a case with 25% larger (52% of vane axial chord) axial spacing and a third case with 25% smaller (31% of vane axial chord) axial spacing.

COMPUTATIONAL PROCEDURES

As details of computational procedures were presented in our previous paper [12], we will only briefly outline them in the following. The HPT model consisted of a stator with 13 vanes and a rotor with 39 blades. To keep the computational geometry as small as possible, we took advantage of the azimuthal periodicity and considered a domain with one vane passage and three rotating blades only.

Figure 1 shows the computational model of the low aspect, transonic HPT. The inlet plane (coloured by red in Fig. 1) was located in the mid-section of a 180 degree curved duct. The outlet plane (coloured by blue in Fig. 1) was located downstream of the rotor exit plane by a distance equal to two blade axial chords in order to reduce possible pressure wave interaction between the rotating blades and the outlet. The front leakage from the secondary air system and the internal cooling passages inside the blades were not modeled but the blade tips were modeled as flat with the ratio of the tip gap height and the blade passage height equal to 0.86%. The aspect ratios of the vanes and the blades were respectively 0.7 and 1.0. These aspect ratios were based on the axial chords at mid span and heights at the trailing edges for the vanes and the leading edges for the blades.

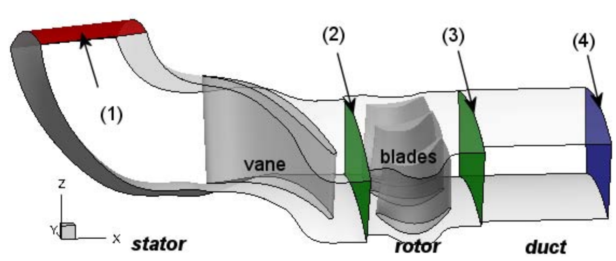

Fig. 1. Computational model of a single-stage high-pressure transonic turbine: (1) inlet; (2) sliding interface between the stator and the rotor; (3) sliding interface between the rotor and the extended duct; (4) outlet.

All simulations have been conducted using the CFD packages FLUENT 6.3 and FLUENT 12. Comparisons between the results using the two versions did not reveal any difference. Considering the compressible nature of turbine flows, the implicit coupled solver was selected. For the spatial and temporal discretization, a second-order upwind scheme and the second-order implicit Euler scheme were used, respectively. Following a review of five different turbulence models (the Spalart-Allmaras, the RNG (Renormalization Group) k-ε, the realizable k-ε, the SST, and the Reynolds stress models (RSM)), the SST model was chosen because of its relatively accurate predictions of compressible flows with adverse pressure gradients or recirculation by comparing to predictions of other two-equation models. The SST model blends the k-ω model in the near-wall region and the k-ε model in the core flow region, as presented by Menter [13]. The use of more accurate models, like the RSM, was not adopted because their computational cost outweighs the possible benefits that come with their use.

The total pressure and the total temperature were specified at the inlet, while the static pressure was specified at the outlet assuming radial equilibrium so that the ratio of the total inlet pressure to the static outlet pressure was 3.5. The turbulence intensity at the inlet was specified as 3% and the hydraulic diameter at the inlet was set at 0.48 m. The rotational speed of the rotor was 49371 rpm. The sliding meshes were used to model the interface regions between the stator and the rotor and between the rotor and the extended duct. Instantaneous solutions were advanced in time using a dual time stepping technique, which accounts for the relative motion of rotor and stator and other sources of unsteadiness. Rotational periodic boundary conditions were employed, based on the assumption that, like the geometry, the velocity distribution was also azimuthally periodic. No-slip and adiabatic conditions were applied to all wall surfaces.

An unstructured mesh was used. It was composed of tetrahedral elements in the core region and prismatic hexahedral elements in the boundary regions, with five prism elements across each boundary region. To reduce the resource requirements, an initial numerical verification was conducted using the mixing plane approach (steady formulation with circumferential averaging between domains) for three meshes, having respectively 1.2, 1.7, and 2.5 million cells. To keep computational resources and time within acceptable limits, mesh adaptation was applied to regions containing shocks and vortices using the pressure gradient so that refined meshes were obtained efficiently. The differences in the degree of reaction were 8.8% between the coarse and the medium meshes, and 1.7% between the medium and the fine meshes. The differences in the turbine stage efficiency were 0.5% between the coarse and the medium meshes, and less than 0.01% between the medium and the fine meshes. This indicates that all three meshes were in the asymptotic range. In addition, we employed the AES (Approximate Error Spline) method suggested by Celik and Li [15] to determine whether the solutions on consecutive grids followed either monotonic or oscillatory convergence. The grid convergence level indices for the coarse, the medium, and the fine meshes were estimated as 14.7, 3.4 and 1.3%, respectively, indicating that an acceptable level of mesh convergence was achieved. It was judged that the medium mesh with 1.7 million cells (0.4 million cells for each blade passage) gave sufficient accuracy for the computation of properties. It may be pointed out, however, that these tests cannot be conclusive, because they utilize steady simulations, which cannot resolve unsteady flow features. For this reason, we conducted additional numerical verifications using unsteady simulations. Comparisons were made between results with coarse and medium meshes only, because our computational resources were not sufficient for unsteady simulations with the fine mesh. The time-averaged total-to-total pressure ratios across the turbine stage were the same for these two meshes. A noticeable difference was in the standard deviation, which was 0.06% for the coarse mesh and 0.5% for the medium mesh. This was attributed to the local mesh adaptation, especially near the trailing edges of the blades and vane. Although some sensitivity of unsteadiness to the mesh resolution was found, the medium mesh with 1.7 million cells was selected, as it gave fair accuracy with relatively low computing time.

The time step was $2\times10^{-3}t_b$ (i.e., 500 time steps were used per blade passing period t_b), small enough to resolve time-varying flow features of interest in the present study. Quantitative tests, based on the discussion by Clark and Grover [16], were also performed to determine the periodic convergence level [12].

Because no appropriate experimental database for the present HPT was available to us, the validation of these specific simulations was only limited. In order to evaluate the selections of schemes and parameter settings as well as the mesh resolution requirement per each passage, we conducted a separate set of unsteady simulations using the TTM single-stage HPT, and validated them against experimental results provided by the Institute for Thermal Turbomachinery and Machine Dynamics (TTM), Graz University of Technology, Austria [17]. The difference between the predicted turbine power and the measured one was 1.7% [14]. Although performed for a different turbine geometry and operating conditions, this validation provided some confidence for our choices of numerical settings and mesh resolution.

COMPUTATIONAL GEOMETRIES

The three axial spacing cases considered included a small gap configuration (31% of the vane axial chord), a nominal gap configuration (42% of the vane axial chord), and a large gap configuration (52% of the vane axial chord).

Figure 2 shows the considered computational geometries focusing on the axial gaps and the rotors. The axial spacing was changed by shifting the rotor axially, while also elongating or shortening the hub and casing sections in the vane domain where the hub and casing endwalls were approximately parallel. This way, the curvatures of the two endwall regions were identical for all three configurations except in the axial gap regions between the vanes and the blades. By doing so, the axial distances between the rotor-stator interfaces and the blade leading edges were the same for all three computational geometries. However, the distances between the vane trailing edges and the interfaces were different because of the differences in the axial lengths of the gap regions.

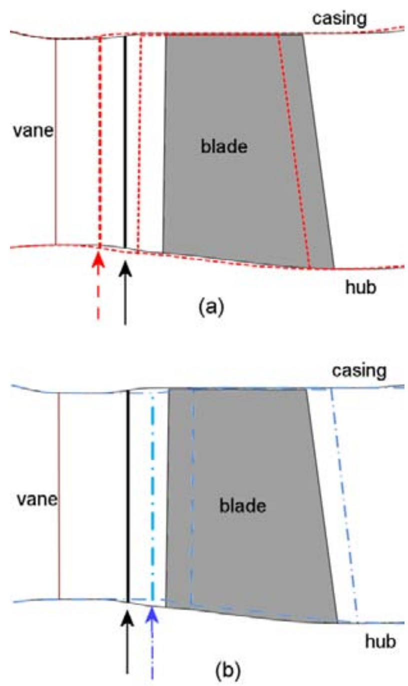

Fig. 2. Computational geometries: (a) nominal gap case (—) vs. small gap case (- - - -) ; (b) nominal gap case (—) vs. large gap case (— · —); arrows mark the stator-rotor interfaces for the three cases.

RESULTS AND DISCUSSION

Instantaneous Flows

In this section, we will present and discuss some representative instantaneous distributions of flow properties, which will be helpful in understanding and explaining the average trends that will be presented in following sections. Instantaneous contours of flow properties will be presented at midspan of the blade, as representative of the overall patterns. Figure 3 introduces a nomenclature of blades according to their relative positions with respect to a corresponding vane, at an instant when the leading edge of the R-blade is aligned with the trailing edge of the vane at 50% span (midspan).

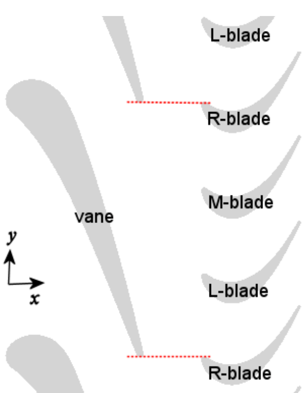

Fig. 3. Reference position at t/t_b = 0.0, when the trailing edge of the vane and the leading edge of the R-blade at 50% span are aligned; dotted lines in red indicate alignment between the trailing edge of the vane and the leading edge of the R-blade.

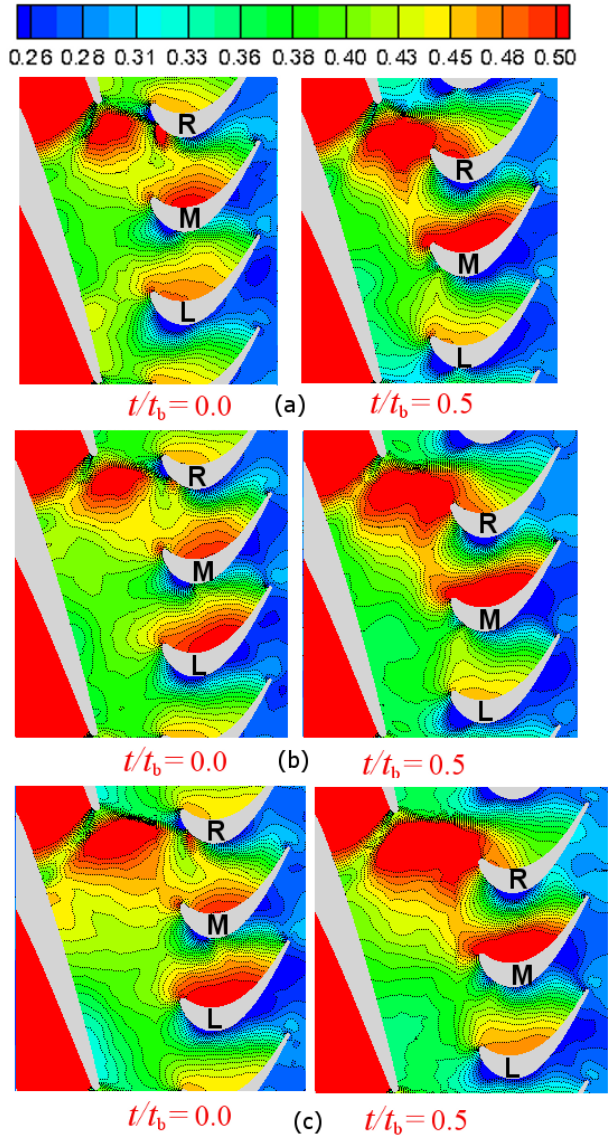

Fig. 4. Instantaneous contours of static pressure, normalized by P_{o1}, at 50% span for the (a) small gap, (b) nominal gap, and (c) large gap cases at t/t_b = 0.0 and 0.5; the rotor motion is from top to bottom and the flow direction is from left to right.

Figure 4 shows instantaneous iso-contours of static pressure, normalized by the total inlet pressure P_{01}, at midspan for two instants. The contour levels were adjusted to illustrate details in the axial gap region. Contours on the left correspond to an instant (t/t_b = 0.0) during which the trailing edge of the vane was aligned with the leading edge of the R-blade as shown in Fig. 3, whereas contours on the right represent an instant (t/t_b = 0.5) half a blade passing period later. Two shock waves are observed to form on either side of the vane trailing edge in all cases. At t/t_b = 0.0, vane shocks from the vane suction side impacted on the R-blade suction side toward the leading edge. At t/t_b = 0.5, these shocks had moved upstream and raised the pressure on the R-blade pressure side toward the leading edge. It is clearly seen in Fig. 4 that, at both times, the high-pressure region just after these shocks increased in size as the gap size was increased.

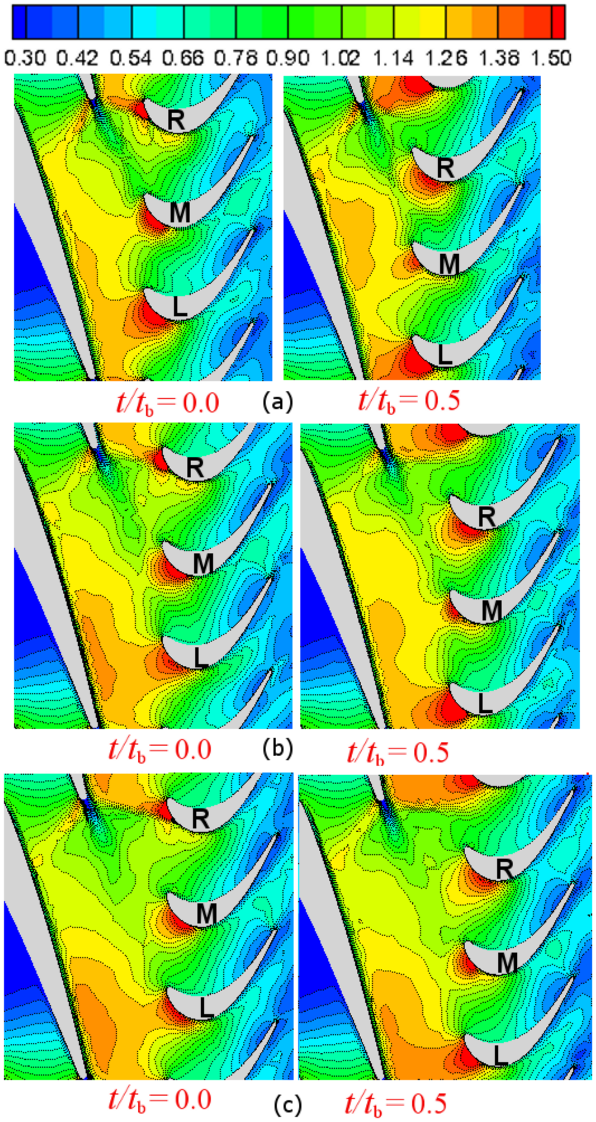

Fig. 5. Instantaneous contours of Mach number at 50% span for the (a) small gap, (b) nominal gap, and (c) large gap cases at t/t_b = 0.0 and 0.5; the rotor motion is from top to bottom and the flow direction is from left to right.

Figure 5 shows instantaneous contours of Mach number at midspan at two instants for all considered cases. The formation of two shock waves at the vane trailing edge was indicated by the sudden decrease in Mach number, which also corresponds to the pressure increase that can be observed in Fig. 4. An increase in the gap size reduced the size of the low Mach number region just after these shocks and increased the local Mach number near the vane suction side toward the trailing edge.

Figure 6 shows instantaneous contours of entropy at midspan, which identify the wakes of the vanes and the blades. In general, during part of the cycle a vane wake impinges on a blade; later it migrates from the pressure side of one blade towards the suction side of the next on-coming blade; and finally, it joins the wake of a blade. As the axial gap size was decreased, the vane near wakes became more distorted by the rotor movement, and the impingement on the blades occurred closer to the wake origin, where the wakes were stronger and thinner. However, the overall effect of the axial gap increase on the average non-uniformity and the turbulence intensity of the flow oncoming upon the blades cannot be assessed by qualitative observations alone, because it is necessary to consider the effects of both the wake width and the wake strength.

Shock waves produce entropy because of high viscosity and heat conduction within the shocks. However, entropy contours in Fig. 6 do not show any visible entropy increase across the shocks. Estimates of the normalized entropy increase across these oblique shocks using Eq. (33) in the article by Denton [19] were of the order of 0.001, which is lower than the contour resolution in these figures. Therefore, it can be concluded that, although the local Mach numbers in the axial gap were relatively high, the vane shocks generated little entropy.

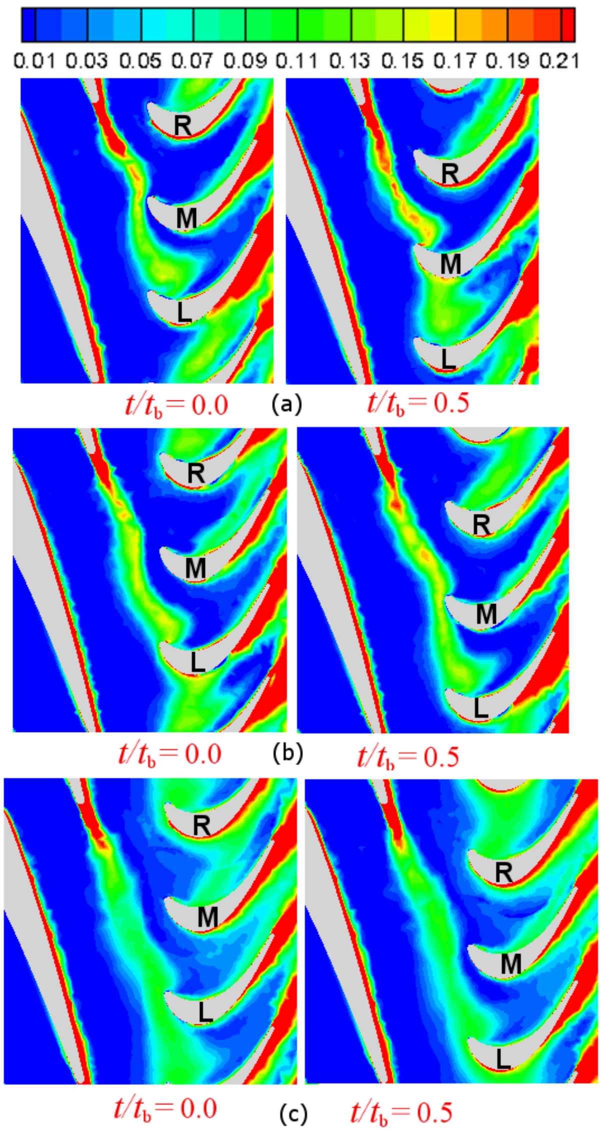

Fig. 6. Instantaneous contours of entropy, normalized by the specific gas constant R, at 50% span for the (a) small gap, (b) nominal gap, and (c) large gap cases at t/t_b = 0.0 and 0.5; the rotor motion is from top to bottom and the flow direction is from left to right.

Time-averaged Flows

In this section, we will first examine time-averaged contours of pressure, Mach number and entropy on the stator-rotor interface plane, which is located at a distance of 21% blade axial chord upstream of the blade leading edges at mid-span. This plane was selected to allow comparisons of results for the three axial gaps at the same location relative to the blades. After that, we will present two pitchwise-averaged spanwise profiles of pressure and Mach number at the stator-rotor interface plane and on a plane located at a distance of 10% blade axial chord downstream of the blade trailing edges at mid-span.

Figure 7 shows iso-contours of time-averaged static pressure, normalized by the total inlet pressure P_{01}, on the stator-rotor interface plane. The dashed lines indicate the vane trailing edges projected on these planes. The ellipses in figures mark vane wakes and show that the local pressure in the wake regions is increased as a result of the corresponding velocity decrease. In all three cases, there is a negative spanwise pressure gradient, which is induced by the vane leaning [17] and is further enhanced by the blade leading edge backward sweeping. In addition, the shocks and the vane wakes generated pitchwise pressure gradients. This figure demonstrates that the pressure gradients increased with decreasing axial gap size and, therefore, that the unsteadiness of the pressure field approaching the blades increased with diminishing axial gap.

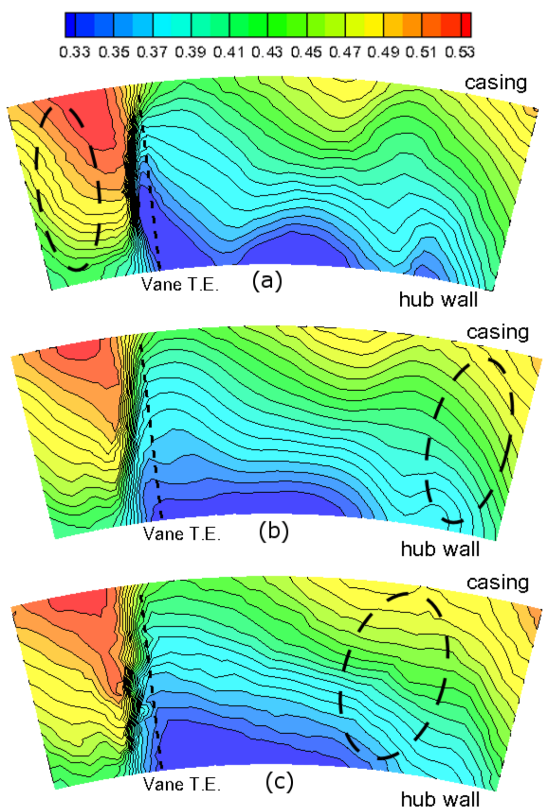

Fig. 7. Iso-contours of time-averaged static pressure P_s normalized by total inlet pressure P_{01}, on the stator-rotor interface plane; dashed lines mark the vane trailing edges projections on the transverse plane; ellipses mark vane wakes; view is towards upstream.

Figure 8 shows iso-contours of the time-averaged Mach number on the stator-rotor interface plane. An increase in Mach number corresponds to a pressure decrease shown in Fig. 7. As the gap size was decreased, the size of high Mach number regions and the Mach number peaks increased near the hub walls toward the vane shocks. It is known that the tangential velocity is the strongest velocity component in these high Mach number regions, where the flow approaches the throat formed by the vane trailing edge and the blade leading edges. These considerations imply that the incidence angle of the flow approaching the blades increased with decreasing gap size. Further considering that the total pressure increases with increasing Mach number, one may conclude that the non-uniformity of the total pressure increased as the gap size was reduced. The low Mach number regions, marked by ellipses in Fig. 8, were due to the vane wakes, which not only reduced the Mach number in the core flows but also increased the boundary layer thicknesses.

Figure 9 shows iso-contours of time-averaged specific entropy on the stator-rotor interface plane, normalized by the specific gas constant. As the gap size was decreased, the vane wake strength increased but the wake width decreased. In addition, decreasing the gap size affected the circumferential positions of the wakes, driving them toward the vane trailing edge projections on the stator-rotor interface plane.

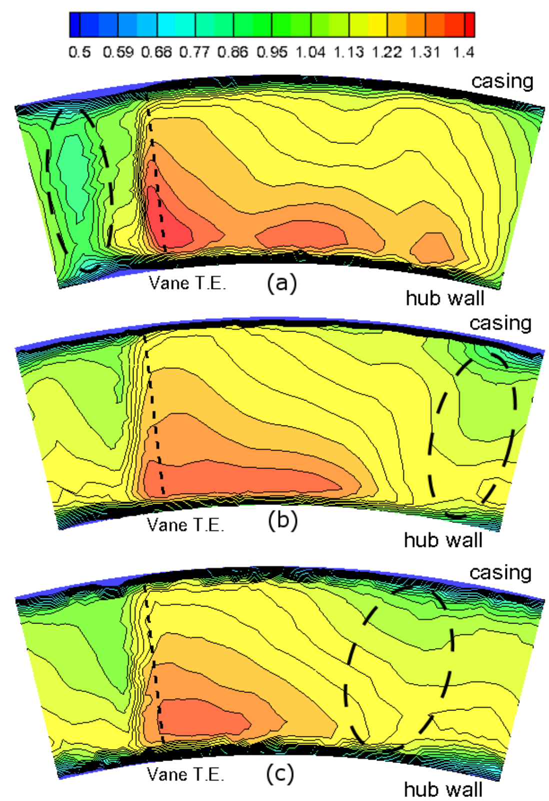

Fig. 8. Iso-contours of time-averaged Mach number M on the stator-rotor interface plane; dashed lines mark the vane trailing edges projections on the transverse plane; ellipses mark low Mach number regions in the vane wakes; view is towards upstream.

By comparing the contours in Figs. 7, 8 and 9, one may conclude that the wakes increased the non-uniformity of the total pressure and the incidence angle of the flow approaching the rotors. Finally, entropy contours show an entropy increase near the endwall regions for both the small gap and the large gap cases. In both cases, this entropy increase may be attributed to interactions between the vane wakes and the endwall boundary layers. For the small gap case, the vane wakes are stronger and cause stronger turbulence in the boundary layers in their vicinity. On the other hand, for the large gap case, the vane wakes are weaker but wider, and therefore, affect wider endwall zones in which they generate turbulence. As a result, one may expect that both the small gap and the large gap cases have higher losses than the nominal case.

Figure 10 shows spanwise profiles of the pitchwise- and time-averaged static pressure normalized by the total inlet pressure P_{01} at two different streamwise locations. On the stator-rotor interface plane, the pressure increased along the span from the hub to the casing wall. The pressure increased with increasing gap size, except in the two endwall regions. As the gap size was increased, the high-pressure region just after the vane shocks increased in size. In the tip region, the pressure for the small gap case was higher than that for the nominal gap case. This could be explained by the stronger shock and high wake strength in the small gap case, which reduced the tangential velocity and increased the pressure. The spanwise profile of pressure on the plane located downstream of the blade trailing edge in Fig. 10 (b) shows that these profiles were relatively uniform. This is the result of the three-dimensional blade design (twisting, leaning, and sweeping of the blades). There were also two low-peaks above and below the 60% span. These indicate the spanwise positions of the rotor casing passage vortices and the rotor hub passage vortices, respectively. The pressures at all spans were comparable for the three considered cases.

Figure 11 shows spanwise profiles of the pitchwise- and time-averaged Mach number at two different streamwise locations. On the stator-rotor interface plane, the Mach number decreased along the span from the hub to the casing wall, except in the two endwall regions. The Mach number in the core flows decreased with increasing axial gap size. In the two endwall regions, the Mach number for both the small gap and the large gap cases was lower than that for the nominal gap case. Similarly to the discussion of entropy contours (Fig. 9) near the endwalls, this decrease of pitchwise-averaged Mach number for the small gap case is associated with increased wake strength, whereas for the large gap case it is associated with increased wake width. Downstream of the blade trailing edge, the relative Mach number increased along the span between 50 and 95% span. This was due to the blade leaning and the action of the Coriolis force, which drives the flow towards the casing [20]. The relative Mach number increased with an increase in axial gap size between 60 and 70% span, whereas in the rest of the span all values were comparable. The relative Mach number decrease with decreasing gap size above midspan may be due to the observed increases in the non-uniformity of total pressure and turbulence intensity, as well as the increase in the incidence at the stator-rotor interface plane; these increases are associated with the strengthening of the vane wakes as the axial gap is decreased. The persistence of HPT vane wake affects beyond the HPT rotor will certainly have some effect on the losses in the space between the HPT and the LPT and possibly the performance of the LPT [10]. As we did not model these LPT regions, we cannot assess such effects in the present study.

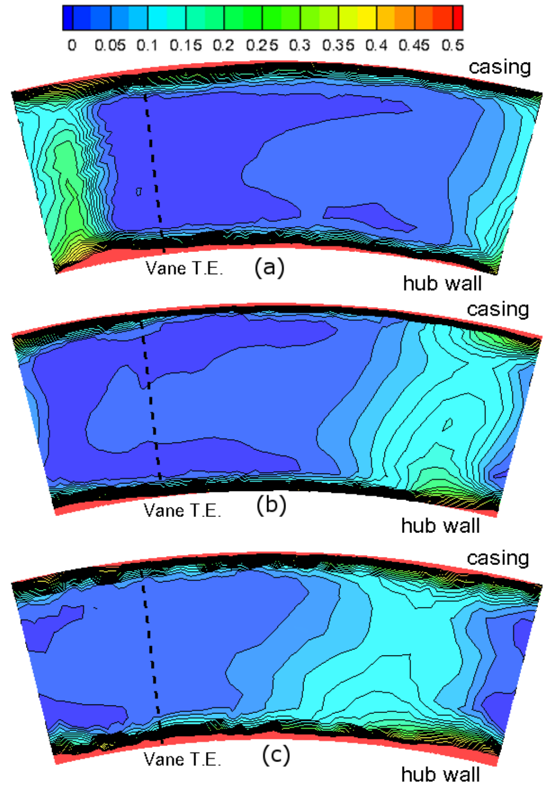

Fig. 9. Iso-contours of time-averaged entropy, normalized by the specific gas constant R, on the stator-rotor interface plane; dashed lines mark the vane trailing edge projection on the transverse plane; view is towards upstream.

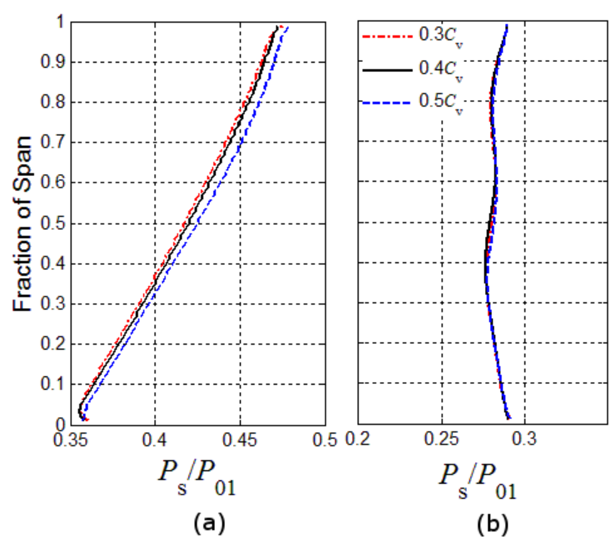

Fig. 10. Time-averaged static pressure P_s normalized by total inlet pressure P_{01}, mass-averaged over planes normal to the turbine axis at axial locations that are upstream of the leading edges of rotor blades by 21% blade axial chord (a) and downstream of the blade by 10% blade axial chord (b); the spanwise position is equal to 0 at the hub and 1 at the casing.

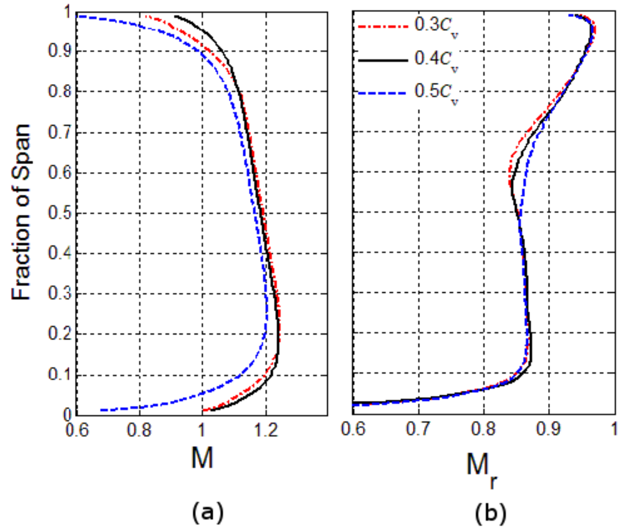

Fig. 11. a) Pitchwise- and time-averaged Mach number, mass-averaged over a plane normal to the turbine axis upstream of the leading edges of the blades by 21% blade axial chord; b) Pitchwise- and time-averaged relative Mach number, mass-averaged over a plane normal to the turbine axis downstream of the blades by 10% axial chord; the spanwise position is equal to 0 at the hub and 1 at the casing.

Pressure Loading on Blade Surface

Figure 12 shows the time-averaged surface pressure normalized by the total inlet pressure at 10, 50 and 90% spans. The time-averaged pressure on the pressure side increased toward the tip (Fig. 10 a), and its maximum shifted toward the leading edge. The effect of axial gap on the time-averaged pressure was small, in agreement with the finding of Venable et al. [4].

Figure 13 shows the standard deviation of surface pressure fluctuations at 10, 50 and 90% spans for three different axial gap sizes. The strongest fluctuations were located on the blade suction side toward the leading edge. The maximum fluctuations decreased along the span for the two larger gap cases, but for the small gap case they were comparable at 10 and 50% spans; thus, the blade surface area where pressure fluctuations were high was larger for the small gap case than for the other cases. The pressure fluctuation maximum decreased with increasing axial gap size [4], as the shocks dissipated in the gap region (see Fig. 7). A reduction in pressure fluctuations with an increase in gap size was also observed at 10% span near the 50% blade axial chord on both the pressure and suction sides. It may be pointed out that increased levels of pressure fluctuations are associated with spatial non-uniformity of pressure, and therefore with reduced turbine performance.

Torque

Figure 14 shows the temporal variation of the blade torque, normalized by the time-averaged torque for the nominal gap case. As the axial spacing was increased, the torque peaks became lower. There were two local peaks before and after the torque maximum in the small gap and the nominal gap cases, but in the large gap case, these local torque peaks were not present. One may relate the specific times at torque peaks to the circumferential position of the blades in Fig. 4: the high torque peaks at t/t_v = 0.5 correspond to the M-blade at t/t_b = 0.5, while the low peaks at t/t_v = 0.0 to the R-blade at t/t_b = 0.0.

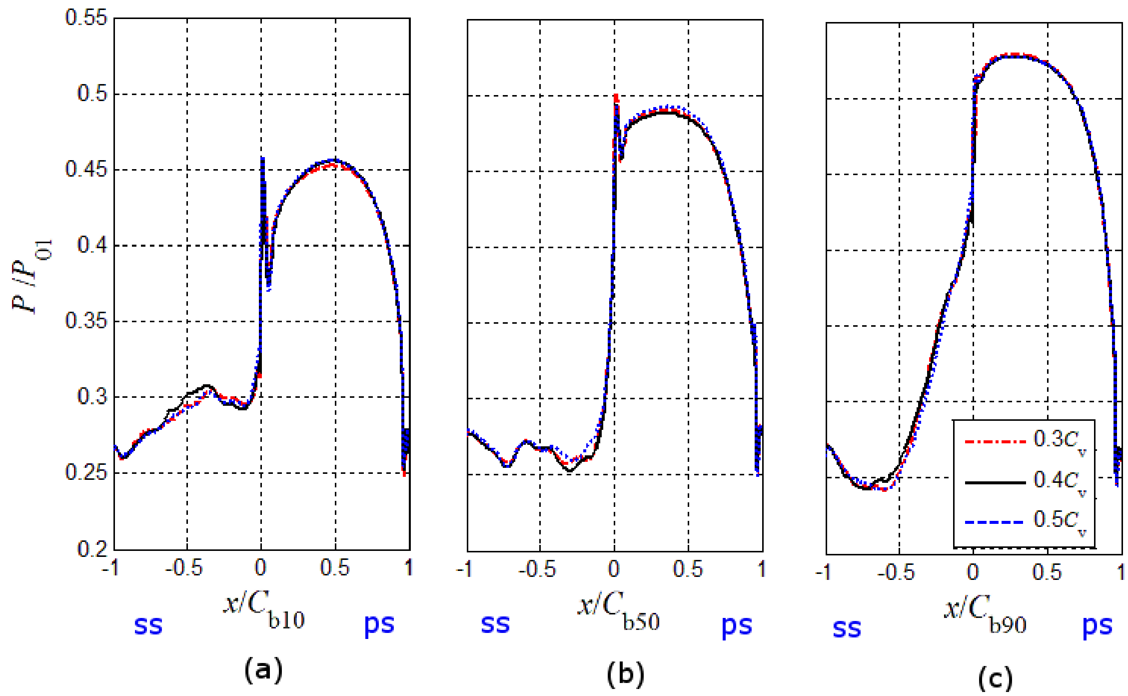

Fig. 12. Time-averaged surface static pressure P_s normalized by the total inlet pressure P_{01} on the blade at 10% span (a); 50% span (b); 90% span (c); x is the axial coordinate; C_{b10}, C_{b50} and C_{b90} are the blade axial chords at 10, 50, and 90% spans; PS is the pressure side of the blade and SS is the suction side; 0 is the leading edge and ±1 is the trailing edge in the normalized axial positions.

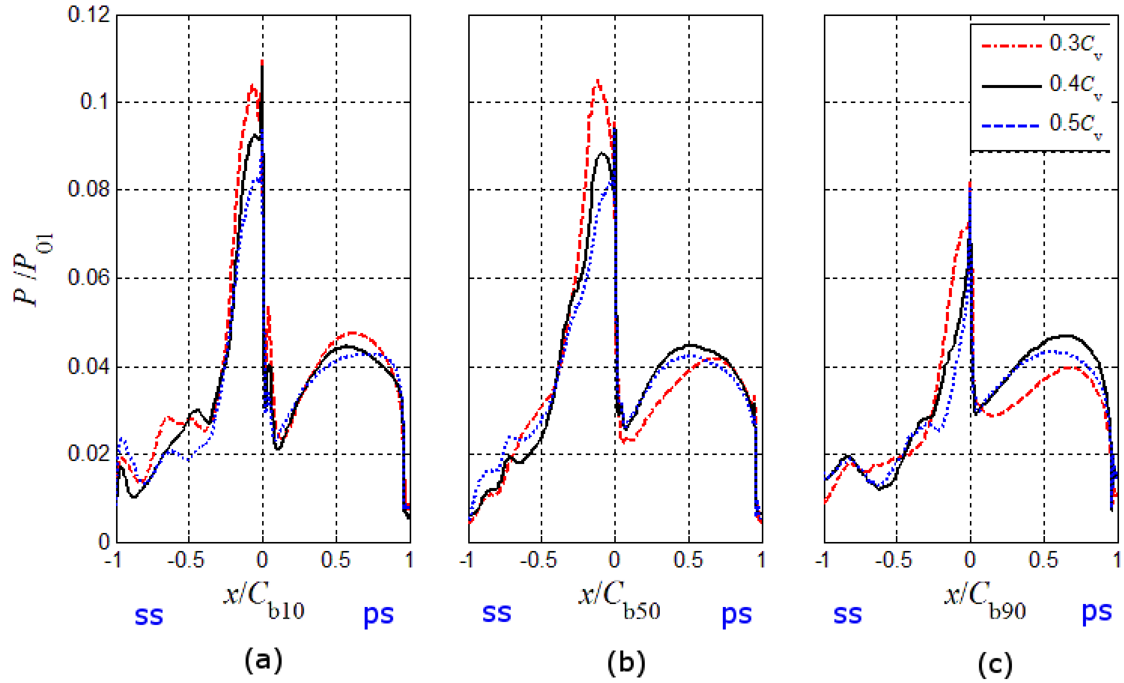

Fig. 13. Standard deviation of surface static pressure P_s normalized by the total inlet pressure P_{01} on the blade at 10% span (a); 50% span (b); 90% span (c); x is the axial coordinate. C_{b10}, C_{b50} and C_{b90} are the blade axial chords at 10, 50, and 90% spans; PS is the pressure surface, while SS is the suction side; 0 is the leading edge and ±1 is the trailing edge in the normalized axial positions.

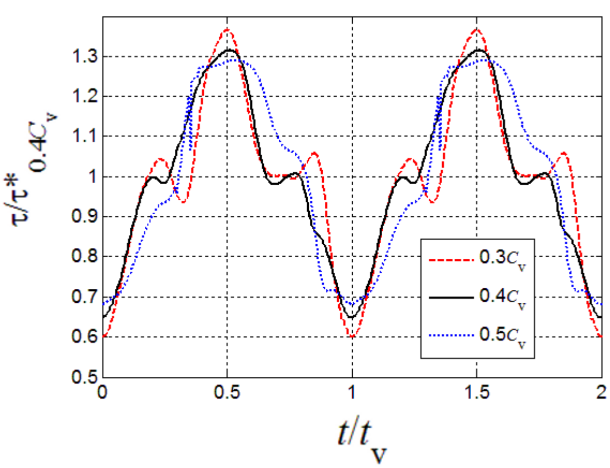

Fig. 14. Time variation of torque τ normalized by the time-averaged torque for the nominal gap case ($\tau^*_{0.4Cv}$); t is time and t_v is a vane passing period.

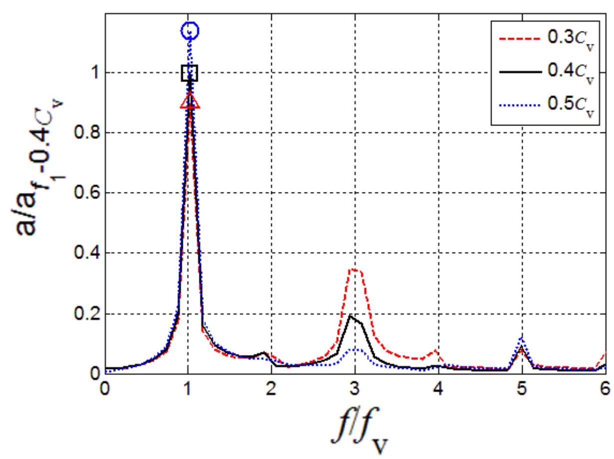

Fig. 15. DFT (Discrete Fourier Transform) magnitude of torque normalized by the DFT magnitude at the fundamental (1st) harmonic for the nominal gap case ($0.4C_v$). The frequency in the abscissa was normalized by the vane passing frequency f_v.

Figure 15 compares the discrete Fourier transform (DFT) magnitudes of the blade torque for the three axial spacing cases. The DFT magnitudes were normalized by the magnitude at the first harmonic for the nominal gap case. As the gap was reduced, the DFT magnitude at the vane first harmonic decreased, whereas the magnitude at the third harmonic increased. The third harmonics are clearly associated with the local peaks in the torque variations (Fig. 14), which became stronger as the axial gap size was reduced. The local torque peaks are the results of a combination of unsteady effects, including vane shocks, vane wakes, reflected pressure waves, vane passage, tip and other vortices and blade shocks, although it is unclear whether one or more of these effects are dominant.

Turbine Performance

Because the specific heat ratio is a function of temperature, the isentropic efficiency of the turbine cannot be determined in an explicit way. Following Denton [19], we defined a turbine efficiency as

$$\eta_{tt} = \frac{\left(\tilde{h}_{01} - \tilde{h}_{03}\right)}{\left(\tilde{h}_{01} - \tilde{h}_{03}\right) + \left[\left(\tilde{s}_3 - \tilde{s}_1\right)\tilde{T}_{03}\right]} \qquad (2)$$

In order to separate the losses in the stator from those in the rotor, the loss coefficient in the stator was calculated as (Pullan et al., [21])

$$\zeta_{\text{stator}} = \frac{\left[(\tilde{s}_2 - \tilde{s}_1)\tilde{T}_{03}\right]}{\left(\tilde{h}_{01} - \tilde{h}_{03}\right) + \left[(\tilde{s}_3 - \tilde{s}_1)\tilde{T}_{03}\right]} \tag{3}$$

where the mass-weighted entropy is $\tilde{s} = \int s\,\rho V dA / \int \rho V dA$, the mass-weighted total enthalpy is $\tilde{h}_0$ and the mass-weighted total temperature is $\tilde{T}_0$. The subscripts 1, 2, and 3 represent the stator inlet, the stator-rotor interface plane, and the rotor outlet, respectively. Similarly, the loss coefficient in the rotor was calculated as

$$\zeta_{\text{rotor}} = \frac{\left[(\tilde{s}_3 - \tilde{s}_2)\tilde{T}_{03}\right]}{\left(\tilde{h}_{01} - \tilde{h}_{03}\right) + \left[(\tilde{s}_3 - \tilde{s}_1)\tilde{T}_{03}\right]} \tag{4}$$

It is obvious that

$$\eta_{\text{tt}} = 1 - \left(\zeta_{\text{rotor}} + \zeta_{\text{stator}}\right) \tag{5}$$

Table 1 compares time-averaged turbine performance parameters, which include the torque, the total-to-total turbine efficiency, the loss coefficient at the stator, and the loss coefficient at the rotor. The values represent percent differences from the nominal gap case; the changes in losses are expressed as percentages of the nominal gap case efficiency. These results indicate that axial gap size changes had a small effect on the torque, but a measurable one on the turbine efficiency and the losses. The nominal gap case had the highest efficiency, and the efficiencies for the smaller and the larger gaps were comparable. This is in agreement with measurements in a subsonic HPT conducted by Gaetani [9]. However, the percent changes of turbine efficiency in this study were different from those found by Venable et al. [4], who reported that the efficiencies for their two larger gap cases were essentially the same and 1% higher than the efficiency for their small gap case.

Table 1 also shows that, for both the small gap and the large gap cases, the losses in the stator were larger than those for the nominal gap case. These loss increases may be attributed to increased turbulence in the endwall boundary layers, as indicated in the discussion of Fig. 9. Moreover, the losses in the rotor were smaller for the large gap case than those for the other two cases. The loss reduction in the rotor for the large gap case may be explained by the improved uniformity of the pressure and the Mach number and the decrease in the flow angle at the stator-rotor interface plane.

Table 1: Time-averaged turbine performance percent differences from the nominal gap case

	$\frac{\Delta\tau}{\tau_{0.4C_v}}$	$\frac{\Delta\eta_{tt}}{\eta_{tt\,0.4C_v}}$	$\frac{\Delta\zeta_{stator}}{\eta_{tt\,0.4C_v}}$	$\frac{\Delta\zeta_{rotor}}{\eta_{tt\,0.4C_v}}$
Small gap case	-0.1	-0.8	+0.7	+0.1
Large gap case	+0.3	-0.9	+1.9	-1.0

CONCLUSIONS

Three-dimensional unsteady Reynolds-averaged Navier-Stokes simulations of compressible flows in a single-stage high-pressure turbine have been performed to investigate the effects of axial spacing between stator vanes and rotor blades on flow features, turbine performance and pressure loading of blades. Three cases have been considered, with axial spacings equal to 31, 42, and 52% of the vane axial chord. The axial gap effects have been examined by comparing instantaneous and time-averaged contours of pressure, Mach number and entropy. It was demonstrated that there were several regions where the local flow parameters were affected significantly by changes in the gap size.

As the gap size was decreased, the pressure in the core flows generally decreased in the gap region, whereas the Mach number increased. Furthermore, decreasing the axial gap size increased the core flow non-uniformity and turbulence as well as the incidence angle of the flow oncoming upon the blades. However, the flows near the two endwalls in the gap region did not follow monotonic trends with the gap size change; instead, the Mach numbers for both the small gap and the large gap cases were lower than that for the nominal gap case. This Mach number decrease was attributed to stronger turbulence in the endwall boundary layers for both the small and the large gap cases.

The effect of gap size was not significant on the time-averaged pressure loading on the blade, whereas it affected strongly the front region of the blade suction side. The case with the smallest gap experienced the strongest pressure fluctuations.

The turbine efficiencies of the cases with the largest and smallest gaps were essentially the same, but both were lower than that of the nominal case with the 42% gap. The stator loss for the small gap case was lower than the one for the large gap case, whereas the opposite was true for the rotor loss.

ACKNOWLEDGMENTS

Financial support for this work was provided by Pratt and Whitney Canada Ltd and the Natural Sciences and Engineering Research Council of Canada.

REFERENCES

[1] Gaetani, P., Persico, G., Dossena, V., Osnaghi, C.: Investigation of the flow field in a high-pressure turbine stage for two stator-rotor axial gaps – part 1: three-dimensional time-averaged flow field. Journal of Turbomachinery, 129, pp. 572-579 (2007)

[2] Dring, R.P., Joslyn, H.D., Hardin, L.W., Wagner, J.H.: Turbine rotor-stator interaction. Journal of Engineering for Power, 104, pp.729-741 (1982)

[3] Koya, M., Kotake, S.: Numerical analysis of fully three-dimensional periodic flows through a turbine stage. Journal of Engineering for Gas Turbines and Power, 107, pp.945-952 (1985)

[4] Venable, B.L., Delaney, R.A., Busby, J.A., Davis, R.L., Dorney, D.J., Dunn, M.G., Haldeman, C.W., Abhari, R.S.: Influence of vane-blade spacing on transonic turbine stage

aerodynamics: part I – time-averaged data and analysis. Journal of Turbomachinery, 121, pp.663-672 (1999)
[5] Busby, J.A., Davis, R.L., Dorney, D.J., Dunn, M.G., Haldeman, C.W., Abhari, R.S., Venable, B.L., Delaney, R.A.: Influence of vane-blade spacing on transonic turbine stage aerodynamics: part II – time-resolved data and analysis. Journal of Turbomachinery, 121, pp.673-682 (1999)
[6] Gaetani, P., Persico, G., Dossena, V., Osnaghi, C.: Investigation of the flow field in a high-pressure turbine stage for two stator-rotor axial gaps – part 2: unsteady flow field. Journal of Turbomachinery, 129, pp. 580-590 (2007)
[7] Kikuchi, M., Funazaki, K-I, Yamada, K., Sato, H.: Detailed studies on aerodynamic performance and unsteady flow behaviours of a single turbine stage with variable rotor-stator axial gap. International Journal of Gas Turbine, Propulsion and Power Systems, 2, pp. 30-37 (2008)
[8] Yamada, K., Funazaki, K., Kikuchi, M., Sato, H.: Influence of axial gap between blade rows on secondary flows and aerodynamic performance in a turbine stage. ASME paper GT2009-59855 (2009)
[9] Gaetani, P., Persico, G., Osnaghi, C.: Effects of axial gap on the vane-rotor interaction in a low aspect ratio turbine stage. Journal of Propulsion and Power, 26, pp.325-334 (2010)
[10] Yao, J., Carson, S.: HPT/LPT interaction and flow management in the inter-turbine space of a modern axial flow turbine. ASME paper GT2006-90636 (2006)
[11] Joslyn, D., Dring, R.: Three-dimensional flow in an axial turbine: part 1-aerodynamic mechanisms. Journal of Turbomachinery, 114, pp. 61-70 (1992)
[12] Chang, D., Tavoularis, S.: Unsteady vortices and blade loading in a high-pressure turbine. ASME paper GT2009-59189 (2009)
[13] Menter, F. R.: Two-equation eddy-viscosity turbulence models for engineering applications. AIAA Journal, 32, pp. 1598-1605 (1994)
[14] Lastiwka, D.: Influence of rotor blade scaling on the numerical simulation of a high pressure gas turbine. Master's Thesis, University of Ottawa, Ottawa, ON, Canada, (2008)
[15] Celik, I., Li, J.: Assessment of numerical uncertainty for the calculations of turbulenct flow over a backward-facing step. International Journal of Numerical Methods in Fluids, 49, pp.1015-1031 (2005)
[16] Clark, J.P., Grover, E.A.: Assessing convergence in predictions of periodic-unsteady flowfields. Journal of Turbomachinery, 129, pp. 740-749 (2007)
[17] Göttlich, E., Neumayer, F., Woisetschläger, J., Sanz, W., Heitmeir, F.: Investigation of stator-rotor interaction in a transonic turbine stage using laser Doppler velocimetry and pneumatic probes. Journal of Turbomachinery 126, pp. 297-305 (2004)
[18] D'lppolito, G., Dossena, V., Mora, A.: The influence of blade lean on straight and annular turbine cascade flow field. Journal of Turbomachinery, 133, 011013, 9 pages (2011)
[19] Denton, J.D.: Loss mechanisms in turbomachines. Journal of Turbomachinery 115, pp. 621-656 (1993)
[20] Ristic, D., Lakshiminarayana. B., Chu, S.: Three-dimensional flow field downstream of an axial flow turbine rotor. Journal of Propulsion and Power, 15, pp. 334-344 (1999)
[21] Pullan, G., Denton J., Curtis, E.: Improving the performance of a turbine with low aspect ratio stators by aft-loading. Journal of Turbomachinery, 128, pp. 492-499 (2006)

